JOURNAL OF MATERIALS SCIENCE **34** (1999) 4023–4030

Liquid phase sintering of RE_2O_3: YSZ ceramics

Part I *Grain growth and expelling of the grain boundary glass phase*

D. P. F. DE SOUZA
Department of Materials Engineering, Federal University of S. Carlos
P.O. Box 676-13 565-905-S. Carlos-SP., Brazil
e-mail: dulcina@power.ufscar.br

M. F. DE SOUZA
Department of Physics and Materials Science, S. Paulo University
P.O. Box 369-13 560-970-S. Carlos-SP., Brazil

Experiments on silicate liquid phase sintering of YSZ ceramics with addition of 0.5 mol % of rare earth ions have been done in order to study the effect of these ions on the kinetics of grain growth and the expulsion of glass through the grain boundaries. Kinetics follow a third power law in the following order YPr > YPrEr > YY > YEr. The expelled glass does not spread over the ceramic grains and its mass is inversely related to grain size. Glass phase separation inside the grain boundaries is found to be a necessary condition for glass expulsion.

1. Introduction

Silica is the most frequently found impurity in zirconia ceramics, mainly in the grain boundaries. Recently, Aoki *et al.* [1] found that a silica concentration as low as 80 ppm decreases the calcia stabilised zirconia grain boundary specific electrical conductivity, σ_{gb}^{sp}. It has been found that small amounts of silica-rich phases migrate along the grain boundaries, concentrating in pockets in stabilised zirconia considered to be of high purity [1, 2]. In systems where the concentration of silicate is considerably higher, sintering proceeds via liquid phase. Silicate liquid phase sintering advantageously decreases the soaking time and temperature of zirconia ceramic sintering. Electrical conductivity, however, decreases mainly due to increased electrical resistance of the grain boundary [3–5]. Gödickmeier *et al.* [6] have studied the effect of intergranular glass films on the grain boundary electrical conductivity of 3Y-TZP ceramics due to additions of SiO_2 and Al_2O_3 in the sintering powders. These authors have found that second phase glass films have Y_2O_3, ZrO_2, Al_2O_3 and SiO_2 in their composition and reach the 1–2 nm equilibrium thickness, as predicted by the theoretical grain boundary thickness calculations of Clarke [7]. Alumina and silica additions, in the molar ratio of 1.0, were found to significantly decrease the grain boundary electrical conductivity and produce a glass phase that spreads along the grain boundaries.

Since silica is always present in commercial zirconia powders and liquid phase sintering is needed for the sintering of several other materials, such as Si_3N_4 [8], an investigation into the sintering of yttria stabilised zirconia through an excess silicate liquid glass phase is proving to be of interest. Moreover, a very frequent procedure is to sinter alumina via liquid phase. Research on the silicate liquid phase sintering [9–11] of alumina and penetration experiments of polycrystalline alumina by glass [12, 13] have provided a better basic understanding of the liquid phase sintering of this material as compared with zirconia. On the other hand, zirconia being an ionic conductor, the changes in its grain boundary capacitance and specific conductivity during liquid phase sintering may provide additional information on the process going on in the glass-ceramic interface. Composition of the liquid phase used for zirconia sintering, in addition to the silicate, includes zirconium and the stabilising ions, the final composition being regulated by the segregation coefficient of each ion between the liquid phase and the zirconia grains. The segregation of aliovalent impurities in the solid state sintering of TZP ceramics has already been recently studied by Hwang and Chen [14]. These authors have shown that segregation is dominated by the space charge present in the grain boundaries.

This paper describes an experimental investigation on the sintering of yttria stabilised zirconia by a silicate liquid phase with controlled minor additions of rare earth ions of different ionic radii, Erbium and Praseodymium. It will be shown that each of those Rare Earth ions have different influences on the sintering process of the ceramic bodies. Their differing segregation behaviour has a strong effect on the expulsion of one separated glass phase during sintering time and on ceramic grain growth.

0022–2461

TABLE I Nominal samples compositions (mol %)

	Y_2O_3	Pr_2O_3	Er_2O_3
YEr	6.5	—	0.5
YPr	6.5	0.5	—
YPrEr	6.5	0.5	0.5
YY	7.0	—	—

In addition each composition has: $0.5Al_2O_3$; $0.12TiO_2$; 0.12CaO; $2.5SiO_2$ (mol %).

2. Experimental

Four different compositions were chosen for this study, all of them essentially the same, differing only in the concentration of the lanthanide elements of different ionic radius. The stabiliser elements of the zirconia phase are Yttrium, Erbium and Praseodymium, whose total molar concentration as oxides in each composition is 7.0 mol %: 6.5% $Y_2O_3 + 0.5\%$ Er_2O_3; 6.5% $Y_2O_3 + 0.5\%$ Pr_2O_3; 6.0% $Y_2O_3 + 0.5\%$ $Er_2O_3 + 0.5\%$ Pr_2O_3; 7.0% Y_2O_3, hereafter referred to, respectively, as compositions YEr, YPr, YPrEr, and YY. The zirconia powder used in this work (TAM Ceramics, USA) already contains additives for silicate liquid phase sintering, but an excess of 1.0 wt % of amorphous silica (Cabosil, USA) was added during powder preparation. The final concentrations of each oxide in the four studied compositions are given in Table I. All the ceramic discs studied were prepared from eight batches, two for each composition. The rare earth starting powders (purity 99.9%, Aldrich, USA) were milled/mixed with zirconia balls (Tosoh-Japan) in polyethylene jars with acetone and 1.0 wt % of PVB (Monsanto, USA). Disc preparation and density measurements were done as already described elsewhere [15]. Final disc diameter after sintering is close to 1.0 cm, while thickness lies between 2.0 and 3.0 mm. Optical microscopy and scanning electron microscopy, SEM, observations were done on polished and unpolished discs in order to examine the glass phase expelled from the discs during sintering, as well as the ceramic microstructure. Energy-dispersive spectroscopy (EDS) quantitative analyses were done in a Zeiss 9600 scanning electron microscope equipped with a microanalizer Link Analytical QX 2000. Only the 8.0 and 16.0 h sintered samples had their grain boundary glass phase analysed. EDS analysis of the concentrations of each oxide in the grain-boundary glass, grains and expelled glass were done on a large number of samples. In order to reduce grain surface interference on the EDS analyses of the expelled glass, the measurements were made on the thicker glass droplets (35 μm). The amount of expelled glass from inside to the surface of the discs during sintering was measured by successive abrasions with a small grain emery paper, weighing and observing the disc surface in an optical microscope. Because the hardness of the glass is lower than that of the zirconia grains, this procedure produced an error under 10% in the mass of the glass phase. In a few discs the height, diameter and angle of the glass drops surface with the ceramic grains, of the larger spots of expelled glass, were measured using a stylus instrument (Talystep, RTHL, England).

3. Results

3.1. Ceramic phase

The microstructures of the ceramic phases show grains with rounded edges typical of liquid phase sintering. One characteristic of the grain boundaries is the alternate structure of glass pockets between thin regions, where the grains maintain closer contact, as shown in Fig. 1A. This is the dominant characteristic of the microstructure of the larger grain size discs, as in the YPr and YPrEr compositions. Regions where the grain boundary was thin between two triple points where also found, as shown in Fig. 1B. This characteristic was found to be more frequent in samples with smaller grain size, as in the discs with the YEr composition. Therefore, the glass phase is located mainly in the junction of more than two grains and in large pockets along the grain boundaries. Most of the thinner parts of the grain boundaries, which contribute significantly to the grain boundary electrical conductivity, are between glass pockets, as shown in Fig. 1A. The fraction of the grain surface area that is in contact with a thin grain boundary, Fig. 1A, was evaluated as follows. It was assumed that these grain boundary thin regions have a circular shape on top of the grain surface. The fraction

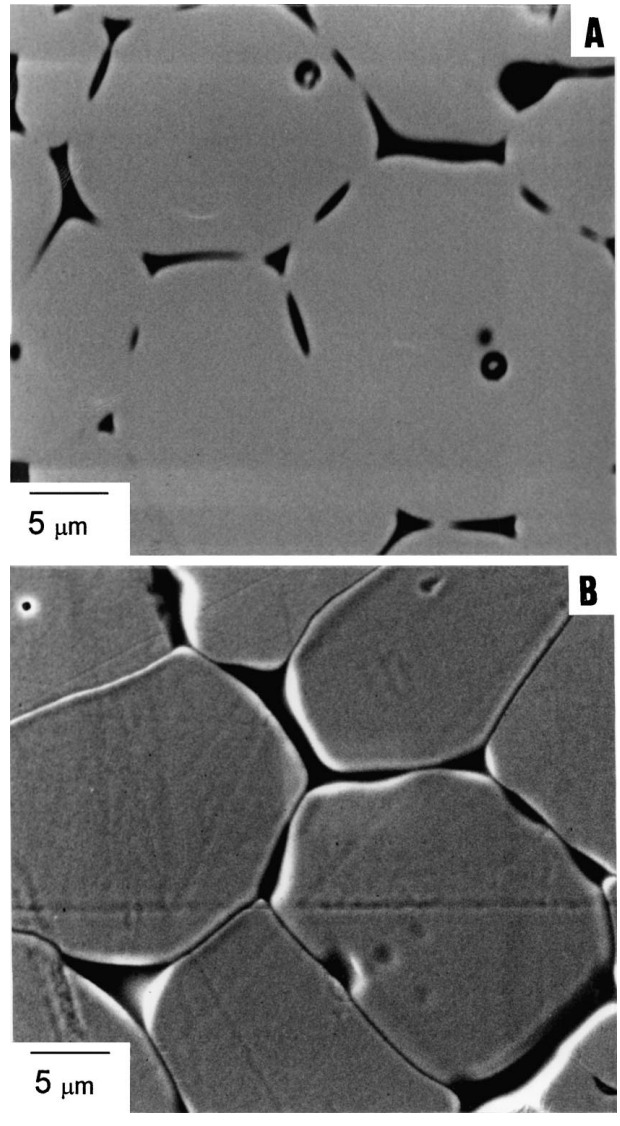

Figure 1 Characteristic microstructure of YPrEr 8.0 h sintered sample: Typical of (A) 75% and (B) 25% of the analysed discs surfaces.

of the area, A, to the total grain surface area, S_g, was estimated from Fig. 1A, to be $A/S_g \approx 25\%$ for the 8.0 h sintered YPrEr discs. The total value for the A/S_g ratio, including both types of microstructure, Fig. 1A and B, was estimated to be approximately 50%. To make this rough estimate, it was taken into account that the microstructures, such as the one shown in Fig. 1B, were found to be present three times less frequently than that shown in Fig. 1A. The microstructures do not have empty pores; the few pores present in the bulk of the grains were filled with glass, some of them aluminium rich. Pores filled with glass with the same composition as the expelled glass were also occasionally found. Sample densities reached a nearly constant value of 5.74 g/cm^3 after the first 0.5 h of sintering, with a very small oscillation of 0.5% around this value. We attribute these variations in density to be due to our experimental method since they were not systematic. The average grain sizes of the sintered discs of the four compositions increased with sintering time, as shown in Fig. 2, in the following order: YEr, YY, YPrEr, and YPr. In the case of all the samples, the first 0.5 h of sintering accounts for nearly half of the final average grain size of the discs. The X-ray diffraction, XRD, detected only zirconia cubic phase in all compositions after 4.0 h of sintering, but samples YEr and YY were already in the cubic phase after 1.0 h of sintering. Although grains with the cubic phase were always present in much larger proportion, few grains with the characteristic tetragonal precipitates were found in some micrographs. The EDS analysis of the grains, grain boundary phases and expelled glass were done on four different discs of each sample composition and three grains in each disc, making a total of twelve analyses for each composition for the same sintering time. The average molar percentages for each oxide in the ceramic grains of the four-studied sample compositions are shown in Table II. This table indicates that Erbium is fully dissolved in the grains after 16 h of sintering, while Praseodymium is only 60% dissolved.

TABLE II Ceramic grain average compositions after 16 h sintering (mol %)

	YEr	YPr	YPrEr	YY
ZrO_2	92.3	92.4	92.4	92.3
Y_2O_3	6.5	6.5	6.0	7.0
Er_2O_3	0.5	—	0.5	—
Pr_2O_3	—	0.3	0.3	—
SiO_2	0.5	0.5	0.5	0.5

Al_2O_3, CaO, TiO_2 = trace.
Maximum deviation: 10%.

3.2. Glass phases

Impurity segregation determined the glass phase compositions, resulting in different properties for the grains and grain boundaries of the ceramic bodies made of the four different compositions. The Praseodymium doped discs expelled a glass phase along the sintering process, Fig. 3, while the YEr composition did not. The distribution on the disc surface of the expelled glass was not uniform, but showed a strong tendency to form glass islands, as shown in the optical micrograph in Fig. 3A. The glass expelled from inside the discs appears on the disc surface around the grains. Further coalescence produced the larger glass islands shown in Fig. 3A and B. To better illustrate glass expulsion, Fig. 4 shows the microstructure of a disc of the YPr composition sintered during 4.0 h at a lower temperature, 1550 °C. The expelled glass is shown around the grains, in the grain boundaries. The observed maximum thickness of the glass islands on the discs sintered at 1610 °C during 8.0 h was 35 μm. The tops of these glass islands were observed to be surrounded by interference Newton rings when a flat glass supported the discs in an inverted optical microscope. The angle θ between the surfaces of the glass and the zirconia grains, at their contact, was found to be near 25° for several droplets.

The amount of expelled glass phase on the disc surfaces, for each sample composition, were measured for several sintering times, as shown in Fig. 5. The mass of the expelled glass has a linear dependence with the inverse of the grain size due to the decrease of the grains total surface area during grain growth (see Fig. 6). Table III shows that the compositions of the expelled glass of samples YPr and YPrEr are the same. Sample YY produced expelled glass, in the form of a few

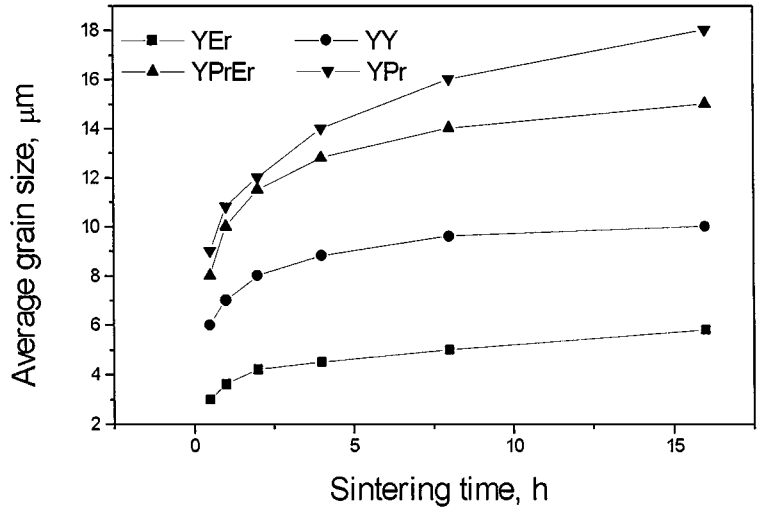

Figure 2 Grain size, d_g, versus sintering time t_s, of the four investigated samples.

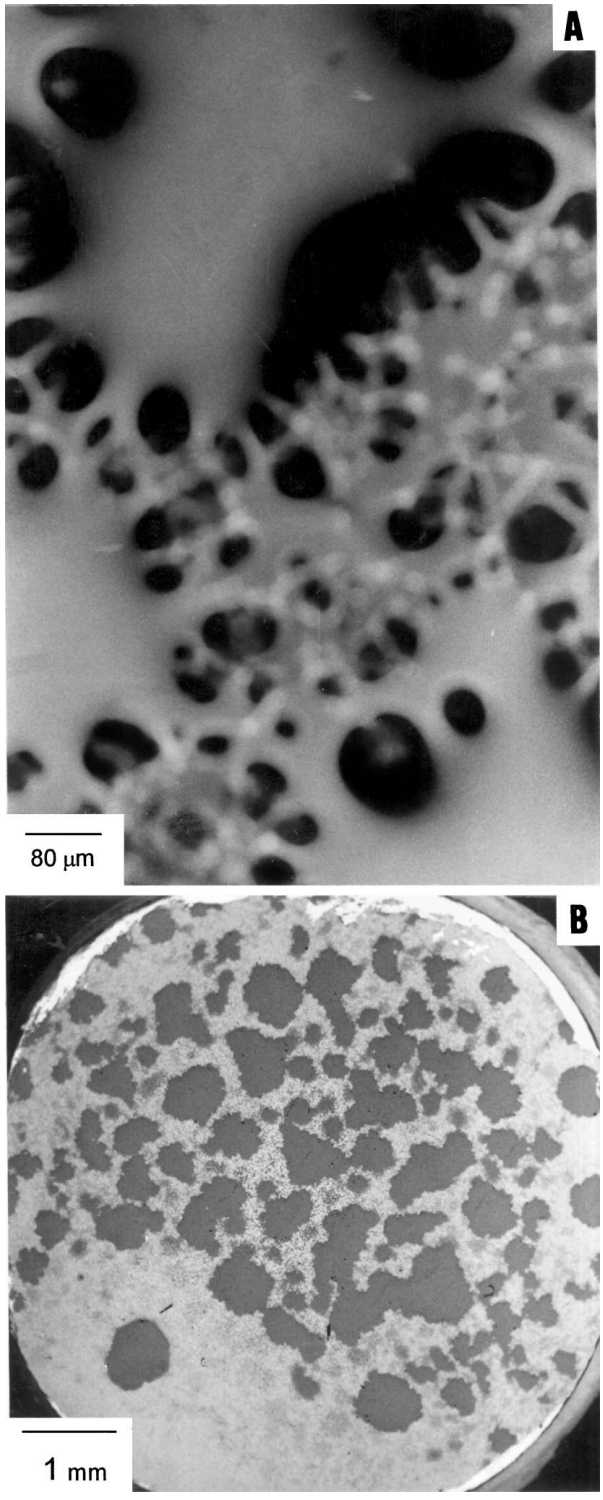

Figure 3 Expelled glass from the YPr sample after 8.0 h sintering: (A) optical microscopy showing details of Fig. 3B; (B) electron microscopy of the same sample.

isolated glass dots, in very small amounts, estimated to be 0.2 mg after 16.0 h of soaking time. Part of the expelled glass from 8.0 h sintered discs of composition YPr left the disc surfaces during sintering. The samples were sintered with their surfaces in an almost vertical position inside a small crucible, their lower part coinciding with the region found to be free of expelled glass. It is presumed that larger glass droplets were accumulated in the lower part, causing them to roll down (see Fig. 1B).

TABLE III Average glass phases compositions (mol %) after 16 h sintering

	Expelled glass (G1)		Grain boundary and pockets glass (G2)			
	YPrEr/Ypr	YY	YEr	YPrEr	YPr	YY
Al_2O_3	10.0	10.5	9.3	9.2	9.0	10.0
CaO	2.1	1.6	1.5	2.1	2.1	1.3
SiO_2	75.4	84.5	73.0	69.0	68.8	75.0
ZrO_2	—	—	7.7	7.0	7.2	5.1
TiO_2	1.0	1.6	1.5	1.1	1.1	1.6
Y_2O_3	5.5	2.6	7.1	6.7	6.7	7.0
Er_2O_3	—	—	—	—	—	—
Pr_2O_3	6.0	—	—	5.0	5.0	—

Error in ZrO_2 and Y_2O_3: ±10%.

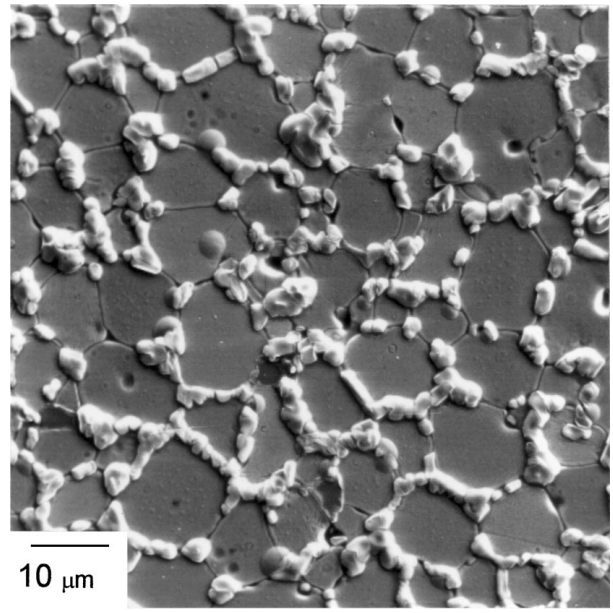

Figure 4 Expelled glass of YPr sample sintered at 1550 °C for 4 h.

The chemical composition of the glass remaining in the grain boundaries, pockets and grain junctions differs from the expelled glass composition, zirconium being present in a larger concentration, as shown in Table III. In several triple points, as well as in a few pockets inside the grains, a larger concentration of silica was found or, in fewer cases, a composition similar to that of the expelled glass. For the sake of simplicity we will call the expelled glass phase the G1 phase, while the one that wets the grains and that remains the discs, will be called the G2 phase. Table III shows the EDS analysis of these glass phases.

The mass of the sintered discs was close to 1.3 g. The maximum amount of expelled glass, G1, of the YPr sample was 5.3 mg, while the mass of the G2 phase was estimated at 52.0 mg. Thus, in our experiments, the expelled glass, G1, was approximately 10 wt % of the total glass phase in the sample. The total mass of glass, G1 + G2, is ≈ 4.4 wt % of the total mass of the disc. As illustrated in Figs 5 and 6, after 8.0 h of sintering the expulsion of the G1 phase of the YPr discs had already been completed, while in the YPrEr discs it was still being expelled at 16.0 h of sintering. The expelled

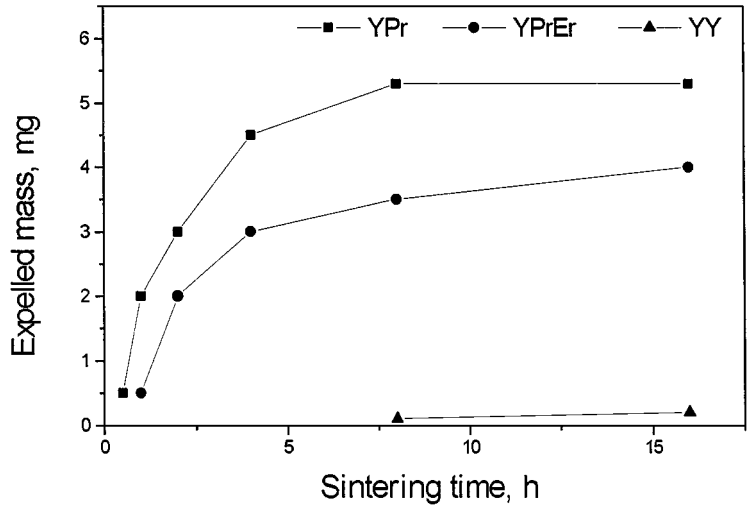

Figure 5 Expelled glass mass versus sintering time, t_s.

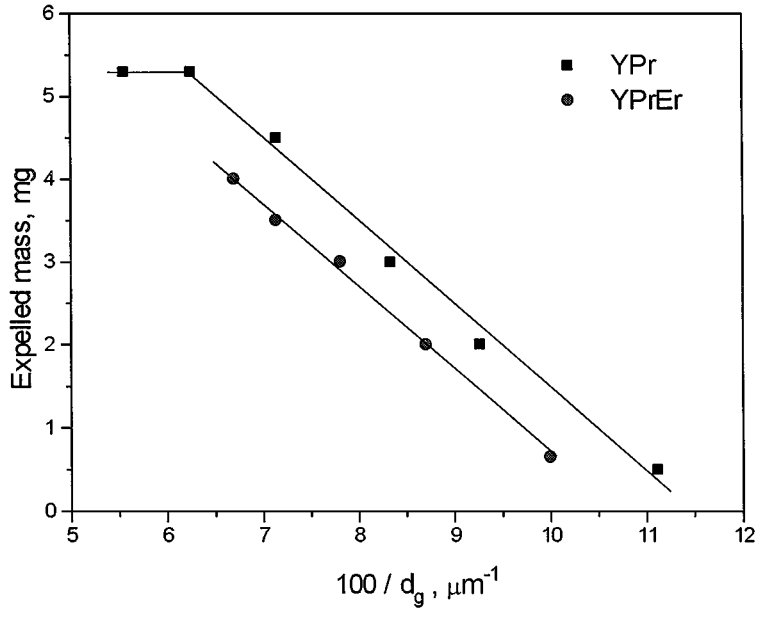

Figure 6 Expelled glass mass versus $100/d_g$.

glass of the YY sample also shows a non-spreading behaviour similar to the G1 phase of the YPr discs. The larger expelled glass dots of the YY discs have a diameter of around 60 μm and are not interconnected.

Although precise segregation coefficients cannot be obtained from our data, it is clear that Erbium has the lowest segregation coefficient, meaning that it is incorporated preferentially into the ceramic grains. Praseodymium shows the opposite behaviour. Yttrium shows approximately the same concentration in the grains and the G2 glass phase of all four studied compositions and is therefore not segregated.

4. Discussion

4.1. Ceramic phase

The microstructures of Fig. 1 show that a large amount of glass phase is distributed along the grain boundaries as a continuous film or in a discontinuous sequence of pockets and thin regions. It is assumed that the equilibrium grain boundary thickness, δ_{gb}, of these thin regions is close to 2.0 nm, as calculated by Clarke [7]. The internal pressure of the liquid phase is not enough to push apart the grains in these thinner regions in order to fully separate the ceramic grains, as happens in penetration experiments [13]. These attracting forces provide a kind of solid skeleton full of the liquid phase in the voids. This arrangement generates the conditions for glass expulsion, as will be discussed in the next section.

The ceramic bodies reached their full density of 5.77 g/cm^3 in the first half hour of sintering. Subsequently, grain coarsening proceeded via liquid phase according to the following Equation [16]:

$$d_g^n - d_0^n = K(t - t_0) \quad (K = 3Dc_0\gamma M/4\rho RT) \quad (1)$$

In the above, d_g is the grain size at time t, d_0 is the grain size at time $t = 0.5$ h and K is a constant dependent on the diffusivity in the medium, D, temperature, T, interfacial energy, γ, solute concentration, c_0, molar mass, M, and density, ρ. The good agreement of our

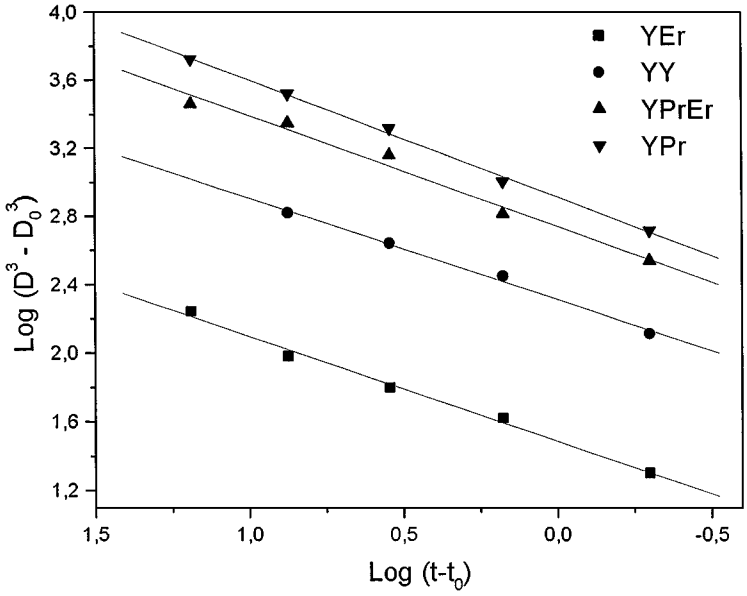

Figure 7 Kinectics of grain corsening.

data for $n = 3$, on a log-log plot, to the above equation is shown in Fig. 7. Agreement in the case of $n = 2$ is poor and the slope deviates from unity. Still from Fig. 7, it is found that K increases in the following order of compositions: YEr < YY < YPrEr < YPr.

The main contribution to this behaviour can be attributed to the difference in diffusivity for mass transport in the glass phases of each composition. Mass transport is associated with the glass viscosity that is dependent on the concentration of nonbridging oxygen, NBO, in the G2 glass phase. It has been shown by Kohli *et al.* [17] that rare earth aluminosilicate glasses contain a broad distribution of NBO types, which increases in concentration with increasing rare earch oxide concentration. Table III shows that the sum of the concentrations of Yttrium and Praseodymium in the G2 glass phase is much higher in the YPr and YPrEr than in the YY and YEr samples. Therefore, diffusivity for mass transport in these compositions must be higher. Although Table III shows differences between the G2 glass phase compositions of samples YY and YEr, they are not so significant as those discussed above. The difference in grain growth between these two compositions must come from the smaller concentration of the Y^{+3} ion in the YEr composition. Therefore, the above results of the effect on the grain growth of YSZ ceramics due to the addition of 0.5 mol % of rare earth elements on 6.5 mol % Y_2O_3 is dependent on the ionic radius of the rare earth ions in an indirect way. In their study of high purity Ce-TZP ceramics with small additions of ions of different ionic radii, Hwang and Chen [14] found that the observed normal grain growth behaviour could be explained using the space charge concept. Build-up of the space charge is dependent on the segregation of the main dopant ion, in the present study of Y^{+3} ion segregation. In this study, grain growth seems to be controlled by the solute transport. Segregation of the Y^{+3} ion will be discussed later in the next section.

Oxide concentration present in the grains after 16.0 h at 1610 °C is shown in Table II. A comparison with Table III shows that Er^{+3} is present only in the grains and has, therefore, not been segregated during grain growth. The same is not true for Praseodymium, which shows a large concentration in the glass phase and a much lower concentration in the grains. Although Praseodymium can produce silicate glasses as a trivalent ion [18], its behaviour could be closer to Cerium that has oxidation states, Ce^{+3} and Ce^{+4}. Considering both these oxidation states for the oxide, the Pr_6O_{11} chemical formula has been proposed. From this formula, the ratio between the concentrations of both valence states is $[Pr^{+4}]/[Pr^{+3}] = 4$. Because the Pr^{+4} ion has a null effective charge in the zirconia lattice and an ionic radius slightly higher than the Zr^{+4} ionic radius, a slight segregation during grain growth could be expected. However, the molar ratio concentration between the G2 glass and the grains is nearly twenty times higher. This result is much closer to the behaviour of a Pr^{+3} ion, which has a larger ionic radius. This study will, therefore, consider only the trivalent state for the Praseodymium ion.

4.2. Glass phase

It is known that a ceramic body fully penetrated by a wetting glass phase keeps its solid form even when the body's volume increases by 50% due to the glass penetration [13]. The reason for this behaviour is the capillary pressure. The total grain surface area decreases during grain growth, causing a redistribution of the glass phase due to local increase of the internal pressure. Transient gradients of pressure are, thus, established inside the body. The final equilibrium pressure is counterbalanced by a change in the wetting angle of the glass on the external surface of the ceramic body. If glass phase separation occurs inside the grain boundary, the droplets of the separated glass will move toward the

external surface of the ceramic body under the action of the gradient of pressure. Pressure gradients are necessary to move separated phases. Hence, the causes for glass expulsion are increased internal pressure due to grain growth and glass phase separation. However, in order to keep the internal gradient pressure, attracting forces between the grains are necessary. These forces are present in the thin regions of the grain boundary.

Fig. 6 shows a linear correlation between the expelled mass and the grain surface. The grain surface area, S_g, relates to grain size, d_g, as $S_g = C/d_g$ [19]. In this equation, C depends on the grain shape and the type of the mean grain size distribution. These two conditions were constants and therefore $S_g \approx 1/d_g$. To look for the separated glass phase a pellet of glass was placed on a YY ceramic disc surface and heated to 1610 °C for 2.0 h in order to allow the glass the penetrate the ceramic disc. The penetrated glass composition is shown in Table IV. After penetration occurred, the disc was sawed perpendicularly to the penetrated surface. Fig. 8 shows the polished surface of the disc where the droplets of the separated glass phase are clearly seen. Thus, the G1 phase was driven out to the disc surface through the grain boundary channels under the pressure gradient generated by the grain growth and opposed by glass viscosity. The YPr and YPrEr sintered disc samples have G1 phases Praseodymium and Yttrium rich that enriched the aluminosilicate glasses NBO, decreasing their viscosities [17]. Their thicker grain boundaries, G1 lower viscosities and large grain size gave these samples a high expelling rate. This allowed the mass expulsion to follow the decrease of grain surface area and therefore to show a linear dependence on $1/d_g$, as shown in Fig. 6. The same figure also shows that the G1 phase of the YPr sample ceased to be expelled after 8.0 h of sintering. The YPrEr composition discs have a smaller grain size when compared to the YPr sample discs. From the above discussion, therefore, it is expected to still be expelling the G1 phase at 16.0 h sintering time. The G1 phase of YY composition is less rich in NBO generating ions (Table III) and must, therefore, have a higher viscosity than the Praseodymium doped samples. Its grain size is also smaller than that of the YPrEr sample for the same sintering time. High viscosity and smaller grain size contribute to decrease the expelling rate of G1 phase of this composition. From our experiments, it cannot be stated conclusively that a glass phase separation did not occur in the YEr samples. The absence of expelled glass from the discs of this composition must be due to the smaller grain size of these samples, which are smaller than the grain size of the YY sample and, therefore, insufficient gradient pressure was generated.

TABLE IV Glass phase composition (mol %) of penetrated glass in YY ceramic disc

Y_2O_3	CaO	Pr_2O_3	Al_2O_3	SiO_2	ZrO_2	TiO_2
5.4	1.9	5.5	9.6	71.8	4.6	1.2

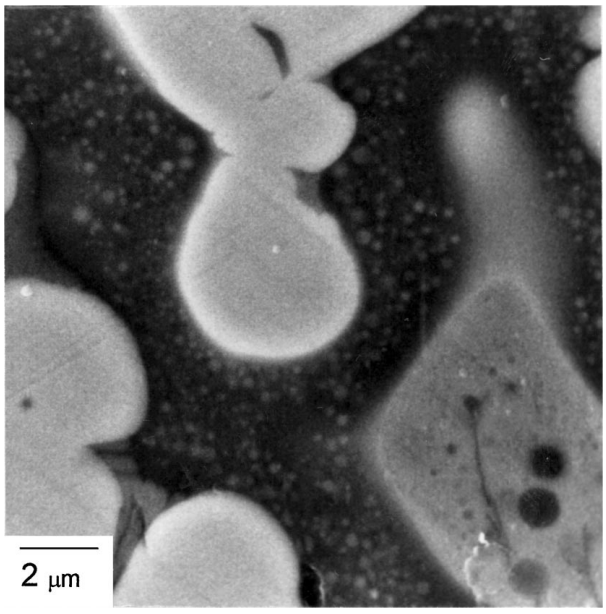

Figure 8 Glass phase penetrated in the YY ceramic disc. Phase transformation is seen as small dots in the dark background.

The properties of all glass phases described in this study are related to their chemical composition, which is shown in Table III. The concentrations of Al_2O_3, CaO and TiO_2 are very similar in all glass phases and, therefore, they do not contribute to the observed difference in their properties. ZrO_2 has a larger concentration in the glasses that wet the ceramic grains, the G2 phases. As for the G1 phase, there is a large difference in Yttrium concentration between the YPr/YPrEr and that of the YY samples shown in Table III. The same table also indicates that the G1 phase of the YY sample is less Yttrium rich than the G2 phase. However, the main difference in composition between the two glass phases is on the zirconia concentration. The measurements of grain and glass compositions after long sintering times give an indication of the segregation behaviour of each ion. SiO_2, Al_2O_3, CaO, and TiO_2 have a higher concentration in the glass phase and a much lower concentration in the grains. Praseodymium shows a much higher concentration in the glass phases, while Erbium is absent. Yttrium shows a peculiar behaviour: its concentration is nearly the same in the grains and the G2 glass phase. Therefore, during the grain growth process, a smaller segregation of the Y^{+3} ion occurs, if any. In the case of null segregation of the Y^{+3} ion, the space charge that develops on the surface of the grains will be determined by the minority stabilising ions. Moreover, grain boundary electrical conductivity is sensitive to grain boundary composition, as will be discussed in part II of this study.

5. Conclusions

The liquid phase sintering behaviour of YSZ ceramics show the following main characteristics:

(1) Third order grain growth kinetics was found to be dependent on the nature of the rare earth doping ion. This dependence is attributed to the different diffusivities in the grain boundary glass phase, introduced by the non-bridging oxygen, NBO, generated by the rare earth ions. Praseodymium was the rare earth found to have

the largest concentration in the glass phase and, therefore, generated the largest NBO concentration. Consequently, Praseodymium doped samples have the fastest grain growth kinetics. The smaller difference in the grain growth kinetics between the YY and YEr compositions can be attributed to other parameters, shown in Equation 1, such as the concentration, c_0, of the Y^{+3} ion and the surface energy, γ.

(2) The large segregation of the Praseodymium ion, as compared with the Er^{+3} and Y^{+3} ions, constitutes strong evidence that, in these experiments, Praseodymium is in the $+3$ oxidation state. The ionic radius of the Pr^{+4}, according to Shannon [20], is very close to that of the Ce^{+4} ion that is highly soluble in the zirconia lattice [14].

(3) The fact that the concentration of the Y^{+3} ion is nearly the same in the grains and in the grain boundary glass, after 16 h of sintering, indicates that Yttrium does not segregate. An interesting consequence of this behaviour is the build-up of the space charge in the grains, as originally proposed by Frenkel [21]. The space charge concept was recently applied by Hwang and Chen [14] to explain the grain growth kinetics of CeTZP ceramics doped with other ions of several ionic radii and valence. Without segregation of the Y^{+3} ion, the build-up of the space charge is determined by the intrinsic defects of the crystalline grains or by minority ions such as the Pr^{+3} and the Ca^{+2} ions. It is a well-known fact that the space charge contributes to increase grain boundary resistivity. Indeed, the compositions studied in this work show different grain boundary electrical properties, as discussed in part II of this paper.

(4) It has been shown that the G1 glass phase is expelled under increased internal pressure generated by reduction of the total grain area. Separation in the glass phase was observed by SEM giving rise to the G1 and G2 glasses. The G1 glass droplets under the gradient of excess internal pressure are squeezed out of the discs through the grain boundary opposed by the friction in the interface with the G2 glass phases. Relaxation of the internal pressure occurred through the G1 mass expulsion. The internal pressure was insufficient to fully separate the grains but sufficient to push out the G1 glass droplets. These droplets start to flow in a lower gradient pressure than the G2 glass through the grain boundaries because the G2 glass wets, preferentially, the grain surface where it must be attached by surface forces. In the absence of the G1 phase and with sufficient liquid phase, the internal pressure will separate the grains, destroying the solid skeleton as happens when the liquid phase penetrates the ceramic body. Phase separation process may cause other effects than glass phase expelling on the grain boundary properties because, during phase separation, each new phase has a composition that differs from the original glass phase in contact with the ceramic grains.

Acknowledgement

The financial support from FAPESP and CNPq are acknowledged.

References

1. M. AOKI, Y. M. CHIANG, I. KOSACKI, L. J. R. LEE, H. TULLER and Y. LIU, *J. Amer. Ceram. Soc.* **79** (1996) 1169.
2. S. P. S. BADWAL and J. DRENNAN, *J. Mater. Sci.* **22** (1987) 3231.
3. S. J. RAGENDRAN, J. DRENNAN and S. P. S. BADWAL, *J. Mater. Sci. Lett.* **6** (1987) 1431.
4. M. J. VERKERK, A. J. WINNUBST and A. J. BURGGRAAF, *J. Mater. Sci.* **17** (1982) 3113.
5. Y. H. KIM and H. G. KIM, *ibid.* **5** (1994) 260.
6. M. GÖDICKMEIER, B. MICHEL, A. ORLIUKAS, P. BOHAC, K. SASAKI, L. GLAUCKER, H. HEINRICH, P. SCHWANDER, G. KOSTORZ, H. HOFMANN and O. FREI, *J. Mater. Res.* **9** (1994) 1228.
7. D. R. CLARKE, *J. Amer. Ceram. Soc.* **70** (1987) 15.
8. C. A. WANG, X. PAN, M. J. HOFFMANN, R. W. CANNON and M. RUHLE, *ibid.* **79** (1996) 788.
9. W. D. KINGERY, *J. Appl. Phys.* **30** (1959) 301.
10. J. E. MARION, C. H. HSUEH and A. G. EVANS, *J. Amer. Ceram. Soc.* **70** (1987) 708.
11. O. H. KWON and G. L. MESSING, *ibid.* **73** (1990) 275.
12. P. L. FLAITZ and J. A. PASK, *ibid.* **70** (1987) 449.
13. T. M. SHAW and P. R. DUNCOMBE, *ibid.* **74** (1991) 2495.
14. S. L. HWANG and I. V. CHEN, *ibid.* **73** (1990) 3269.
15. D. P. F. DE SOUZA, A. L. CHINELATTO and M. F. DE SOUZA, *J. Mater. Sci.* **30** (1995) 4355.
16. Y. M. CHIANG, D. BIRNIE III and W. D. KINGERY, in "Physical Ceramics, Principles for Ceramic Science and Engineering" (John Wiley & Sons, New York, 1997) p. 391.
17. J. T. KOHLI, R. A. CONDRATE and J. E. SHELBY, *Physics Chem. Glasses* **33** (1993) 81.
18. G. DE, A. LICCIULLI and M. NACUCCHI, *J. Non-Cryst. Solids* **201** (1996) 153.
19. M. I. MENDELSON, *J. Amer. Ceram. Soc.* **52** (1969) 443.
20. R. D. SHANNON, *Acta Cryst.* **A 32** (1976) 751.
21. J. FRENKEL, in "Kinetic Theory of Liquids" (Oxford University Press, New York, 1946) p. 36.

Received 9 April
and accepted 25 November 1998